Active Antenna Array Behavior

Denver E. J. Humphrey, *Student Member, IEEE*, Vincent F. Fusco, *Member, IEEE*, and Stephen Drew

Abstract—**It has been recently demonstrated that arrays of coupled active antenna oscillating elements can be locked together by mutual radiation in order to form spatial power combining and beam steered arrays. In this paper a nonlinear coupled oscillator theory is developed which accounts for both the amplitude and phase behavior of an array of distributed coupled active antenna oscillators. In its canonical form the theory can be used to describe the behavior of any number of spatially displaced coupled elements placed in a chain. These elements can have unequal spacing and they can have arbitrary free-running oscillation frequencies. Unequal free-running amplitudes are also permitted. Experimental validation of the theory is presented for some basic cases in terms of frequency and amplitude variation under mutual injection locked conditions. In its particular form the theory developed is suited for use with recently reported active antenna imaging methods.**

I. Introduction

IT IS known that mutual coupling between active antennas can cause injection locking [1], [2] to occur. A lumped element circuit based analysis for the synchronization of the phases of several coupled oscillators was given by Stephan [3]. Modal stability was discussed for lumped element coupling by Endo and Mori [4] and for distributed coupling by Nogi *et al.*[5], and Lin and Itoh [6] while York and Compton have described the phase dynamics of active antenna oscillator circuits with delayed coupling [7]. Arrays of coupled active patch oscillator circuits offer potential for beam scanning applications which do not require phase shifters [8]. Other applications include spatial power combining circuits [9], [10]. Normally the theoretical treatment of these systems concentrates on phase variation effects only. In the work presented here both amplitude and phase variation are permitted.

Several methods for modeling the behavior of a single active antenna element exist. The first method relies on a detailed time domain based simulation of the physical active antenna circuit. In this approach a time domain circuit simulator is used to accurately mimic the electrical characteristics of a given active antenna circuit. A small number of coupled active antenna oscillators have been simulated by this method [10]. For the work presented here, the active antenna circuit used utilizes an NEC71084 MESFET device as the active element and is designed in accordance with the details given in [11]. Microwave Spice is used as the nonlinear time-domain simulator with the active antenna described using the transmission line model given in [12]. For array studies a simpler model customized to the performance characteristics of the full model is more attractive primarily due to the complexity and computational requirements of a multiple oscillator circuit scenario required by the full time-domain modeling strategy. In the work reported here a simple circuit model for the active antenna model is selected. The model can be described by a modified Van der Pol equation [13]. The form of this model is chosen by investigation of the behavioral characteristic of the full time-domain simulation of a single element. The Van der Pol model has appropriate dynamical behavior to allow it to behave with the same amplitude and frequency characteristics as the more complex time-domain model from which it is derived. The justification for the selection of the particular form of the Van der Pol model used is given.

Manuscript received May 16, 1994; revised April 24, 1995. This work was supported in part by the Department of Education for Northern Ireland and EPSRC GR/J40171.

The authors are with the High Frequency Electronics Laboratory, Department of Electrical and Electronic Engineering, The Queen's University of Belfast, Belfast, BT9 5AH, N. Ireland, U.K.

IEEE Log Number 9412691.

II. Active Antenna Element

Fig. 1 illustrates the series feedback oscillator configuration of the active element used in this work. For a nominal operating voltage for the circuit of three volts with a drain current of 35 mA, the radiation patterns obtained for the patch exhibit good symmetry and are compatible in form with those obtained from a radiating-edge fed single passive patch radiator operated in T_{01} mode [14], Fig. 2. A worst case cross polarization level was calculated to be -10 dB, with a measured value of -8 dB. This level of cross polarization is commensurate with the reduction (when compared with radiating edge fed patch variants) in cross polarization normally experienced in nonradiating edge fed passive rectangular microstrip patch antennas [15]. The free-running frequency of the element was 10.67 GHz and its EIRP was 12 dBm. For the active antenna element, both output power and operating frequency are a function of the dc bias voltage applied to the element. The oscillation frequency of the module changed by 30 MHz over the voltage range 2–3 V. Over this voltage range the output power varied monotonically by -3 dB relative to the nominal reference level 12.0 dBm @ 3 V dc bias.

III. Active Antenna Macro Model

The microstrip patch antenna transmission line circuit model [12] used in the full time domain circuit simulator described in [11] was replaced by a variable amplitude sinusoidal voltage source, $v(t) = v$, placed at the device plane AA′ in Fig. 1. At the free-running frequency of the oscillator the input admittance characteristic of the active antenna simulated at this drive port (considered in this work to be the device plane) was found. Fig. 3 shows the functional nonlinear IV form

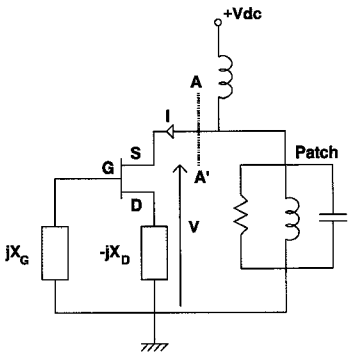

Fig. 1. Active antenna electrical circuit schematic.

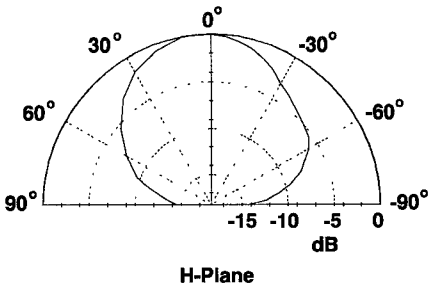

Fig. 2. Far-field H-plane polar pattern for single active antenna module.

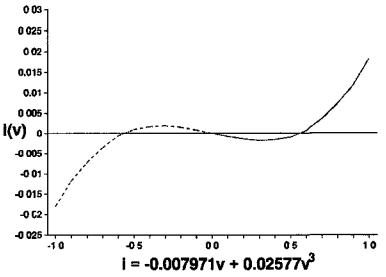

Fig. 3. Simulated nonlinear IV relationship at the device plane at AA′ of Fig. 1.

obtained. This relationship was modeled using the classical cubic relationship for nonlinear conductance required for the formation of a sinusoidal oscillator limit cycle [13]

$$i = -av + bv^3. \tag{1}$$

The derivative of this expression gives the nonlinear conductance for the active antenna element

$$G(v) = \frac{di}{dv} = -a + 3bv^2. \tag{2}$$

Using the full time domain simulation, it was found that at the active antenna free-running frequency, the input reactance of the microstrip patch antenna was inductive. Under the same operating conditions the reactance looking toward the oscillator element at the reference port was found to be capacitive. Over the range of voltage to be fitted by (2) this capacitance was found to be insensitive to voltage drive level.

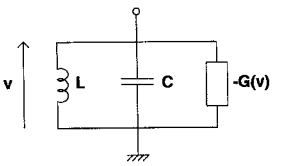

Fig. 4. Single active antenna macro model topology.

From the above information the simple autonomous oscillator circuit topology in Fig. 4 was defined. For the rest of the work presented here the topology in Fig. 4 is used as the macro active antenna model for each element in the chain array.

The simulation approach adopted here justifies the simple model normally assumed arbitrarily in coupled oscillator studies. In addition it yields the numerical circuit values needed to customize the model to the active circuit. On applying Kirchoff's current law to Fig. 4 under free-running conditions, (3) is obtained

$$\ddot{v}(t) - \varepsilon[1 - \beta v(t)^2]\omega\dot{v}(t) + \omega^2 v(t) = 0 \tag{3}$$

where

$$\varepsilon = \frac{a}{C\omega};$$
$$\beta = \frac{3b}{a};$$
$$\omega^2 = \frac{1}{LC}.$$

This equation has the form of a modified version of the classical Van der Pol equation [13].

On application of the averaging method [16] a first order analytical solution for (3) can be obtained.

With initial conditions $v = A$, $\dot{v} = 0$ at $t = 0$ the solution given in (4) results

$$v(t) = A\cos\omega t + 3\frac{\varepsilon A}{8}\sin\omega t \tag{4}$$

where all second order terms have been assumed to be zero.

It should be noted that to achieve a nontrivial solution to (3) the free-running amplitude of the active antenna must equal $A = \sqrt{4/\beta}$. Also since ε is small, 0.025 in this case, the active antenna oscillator exhibits very low harmonic content. This implies that a measurement of the free-running amplitude of the active antenna can be used to find β directly. In this way the need for the full nonlinear computer modeling approach used above to ascertain the correct functional form for the macro circuit can be circumvented.

Examination of the quality factor Q for the circuit in Fig. 4 reveals that

$$Q = \frac{C\omega}{a} = \frac{1}{\varepsilon}. \tag{5}$$

A direct measurement of the active antenna oscillator Q factor will yield ε without recourse to simulation, ε was found by measurement to be 0.027 by injection locking [17] and calculated to be 0.025.

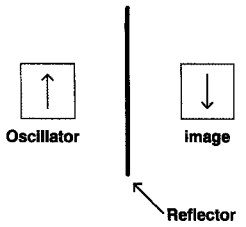

Fig. 5. Imaged active antenna array topology.

IV. Image Coupled Active Antenna Array

Stephan and York [18], and York and Compton [1] suggest a method whereby an active antenna element was imaged onto a vertical ground plane. This enabled the complex coupling coefficient that exists between an active element and its image to be found. The method proceeds by monitoring the frequency of oscillation of the active antenna as a vertical ground plane is moved relative to the active element under test. The resulting shift in frequency induced by load pulling was then used to determine the coupling coefficient.

In this paper, unlike previous analyses—phase and amplitude behavior are considered in a coupled manner. For an imaged active antenna, Fig. 5, the amplitude and free-running frequencies of both the antenna and its image will be identical as will the Van der Pol amplitude factor β and dissipation factor ε for each oscillator, actual and image. The image will be either in-phase or in anti-phase depending on whether E or H plane coupling is used [1]. The coupling $\lambda = \rho e^{j\Phi}$ between the active antenna and its image is assumed to be complex and reciprocal. It is noted that the coupling analyzed in this paper is such that the output of one oscillator directly effects the output of the next oscillator, first and second derivative coupling have been neglected, thereby modeling the single stable limit cycle condition observed experimentally in this paper. Under these constraints (3) can be recast for the active antenna voltage v_1 and the image voltage v_2 as

$$\begin{aligned} \ddot{v}_1 - \varepsilon[1 - \beta(v_1 + \lambda v_2)]^2 \dot{v}_1 \omega + \omega^2 (v_1 + \lambda v_2) &= 0 \\ \ddot{v}_2 - \varepsilon[1 - \beta(v_2 + \lambda v_1)]^2 \dot{v}_2 \omega + \omega^2 (v_2 + \lambda v_1) &= 0 \end{aligned} \quad (6)$$

with the assumed solutions

$$\begin{aligned} v_1 &= A_1 \cos(\omega_L t) \\ v_2 &= A_2 \cos(\omega_L t + \alpha). \end{aligned}$$

Here A_1 is the steady state peak amplitude of the active antenna and is a function of separation distance x. A_2 is the image amplitude and is equal to A_1. The entrained radian frequency of the array which is assumed to be in-lock due to mutual injection locking between oscillator and image is ω_L. In the imaged case, the phase shift, α, between the active antenna and its image must be either 0° or 180° in order for a nontrivial solution of (6) to occur. Here for the purpose of illustration, H-plane coupling is used making $\alpha = 180°$, [1]. The simultaneous in (6) are solved by the analytical harmonic balance approach [16], [19]. Due to the Q-factor

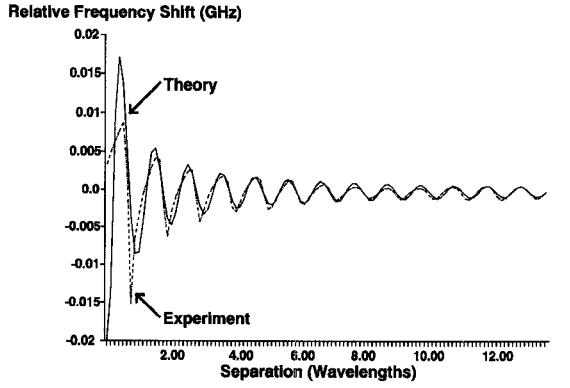

(a)

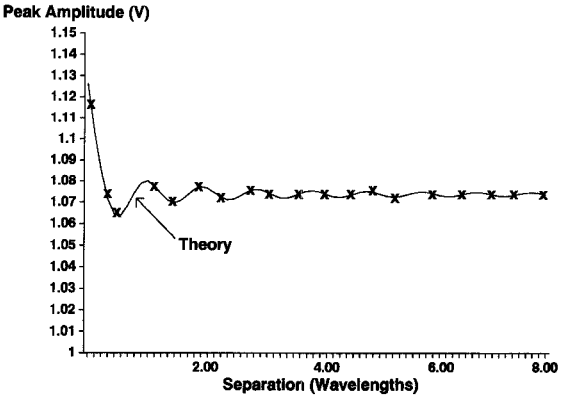

(b)

Fig. 6. (a) Frequency deviation about free-running frequency for a imaged active antenna. (b) Amplitude variation for an imaged active antenna.

of the active antenna element, single frequency operation is assumed, and we thus consider only fundamental frequency terms. This procedure after cosine and sine terms are equated, results in (7)

$$\omega_L = \frac{k}{\varepsilon}\left[\frac{1}{2} + \rho^2\left(1 - \frac{1}{2}\cos 2\Phi\right) - \rho\cos\Phi\right] - \frac{\omega}{\varepsilon}\rho\sin\Phi$$

and

$$\omega_L^2 = k\omega\left(\frac{\rho^2}{2}\sin 2\Phi - \rho\sin\Phi\right) + \omega^2(1 - \rho\cos\Phi) \quad (7)$$

where $k = (A^2\varepsilon\beta\omega_L/2)$ and $A_1 = A_2 = A$.

These two equations in two unknowns A and ω_L can be directly solved for a known antenna element separation. In the free-running oscillator case, i.e., when $\lambda = 0 (\rho = 0)$ (7) suggests $A^2 = 4/\beta$ which is the same result as that obtained from the first order analytical solution for the free-running oscillator, (4). In addition when $\lambda = 0$ the entrained frequency, ω_L, becomes the free-running frequency, ω, as expected.

Experimental and theoretical results are presented in Fig. 6(a) for the frequency deviation of the system relative to the free-running frequency of an individual element as a function of element separation for the image configuration shown in Fig. 5. Here the empirical amplitude coupling coefficient $C = (2\pi x\rho/\lambda)$, [1], is obtained as 0.01209 by numerically fitting (7) at a single arbitrarily selected separation

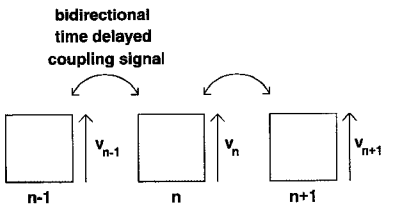

Fig. 7. Chain array topology.

distance of $(x/\lambda) = 5.55$. In Fig. 6(b) theoretical amplitude variation is shown for the imaged antenna and is compared with the amplitude variation measured at the patch. Here power readings were made through a bias tee connected to the element's dc port. These values were then normalized to the peak-peak theoretical amplitude prediction.

V. Chain Array

The basic equation used for individual oscillator cells (delayed coupled active antenna modules in this case) is of the Van der Pol type as given in (3). This equation can be written in canonical form as

$$\ddot{v}_n - \varepsilon_n[1 - \beta_n(v_n + \lambda_{n-1}v_{n-1} + \lambda_n v_{n+1})^2]\dot{v}_n\omega_n + \omega_n^2(v_n + \lambda_{n-1}v_{n-1} + \lambda_n v_{n+1}) + \text{forcing } fn = 0. \tag{8}$$

Where for generality, ε_n and β_n are different for each of the active antenna oscillator modules in the chain array defined in Fig. 7. In this way, unequal active antenna oscillating characteristics and element spacings can be accommodated.

For array behavior to be investigated, the forcing function is assumed to be zero. Again a solution is expected of the form $v_n = A_n \cos(\omega_L t + \alpha_n)$.

In (8) the constant λ_{n-1} is defined as the coupling coefficient between the current and previous oscillator and λ_n is the coupling coefficient between the current and next oscillator. In general, these can be unequal for nonuniformly spaced elements. Only nearest neighbor coupling is accounted for since these are the strongest couplings and will tend to dominate system behavior.

As before a phase lag, Φ_{jk}, is introduced into the coupling mechanism due to the spacial separation of the elements in the array, so that

$$\lambda_{jk} \equiv \rho_{jk} \exp(j\Phi_{jk}). \tag{9}$$

In most arrays reciprocity will hold so that the coupling will be equal in both directions [1]

$$\lambda_{jk} = \lambda_{kj}. \tag{10}$$

Introducing a phase lag, Φ, into the terms $\lambda_{n-1}v_{n-1}$ and $\lambda_n v_{n+1}$ these become

$$\lambda_{n-1}v_{n-1} = \rho_{n-1}A_{n-1}\cos(\omega_L t + \alpha_{n-1} + \Phi_{n-1}) \tag{11}$$

$$\lambda_n v_{n+1} = \rho_n A_{n+1}\cos(\omega_L t + \alpha_{n+1} + \Phi_n). \tag{12}$$

Here ω_L is the entrained frequency of the system and α_n is the phase of the nth oscillator in the system. It is noted that for identical element separations both the magnitude and the phase of the coupling coefficient, λ, (9), will change depending on whether the situation being considered is for two identical oscillators or for a single oscillator and its image. The differential equation describing the general behavior of the chain array, (8), with the substitutions defined by (11) and (12) was solved by application of the method of analytical harmonic balance, [16], Appendix.

1) Solution 1—Two-element array: Consider an array of two oscillator elements. Here the entrainment condition can be assumed to be of the form

$$v_1 = A_1\cos(\omega_L t) \tag{13}$$

$$v_2 = A_2\cos(\omega_L t + \alpha_2). \tag{14}$$

The phase difference between oscillators, $\alpha_2(\alpha_1 = 0)$, is measured relative to the first oscillator. Coefficients A_1 and A_2 represent the steady state amplitudes of the entrained active elements for a given element separation. From (A1) and (A2), (15) and (16) for the first element and (17) and (18) for the second element result

$$-A_1\omega_L^2 - \frac{\varepsilon_1\beta_1\omega_1\omega_L\rho^2A_1A_2^2}{2}\cdot\left[-\frac{1}{2}\sin 2\Phi_1\cos 2\alpha_2 - \frac{1}{2}\cos 2\Phi_1\sin 2\alpha_2\right] + \frac{\varepsilon_1\beta_1\omega_1\omega_L\rho A_1^2A_2}{2}\sin(\alpha_2 + \Phi_1) + \omega_1^2A_1 + \omega_1^2\rho A_2\cos(\alpha_2 + \Phi_1) = 0 \tag{15}$$

$$\varepsilon_1\omega_1A_1\omega_L - \frac{\varepsilon_1\beta_1\omega_1\omega_LA_1^3}{4} - \frac{\varepsilon_1\beta_1\omega_1\omega_L\rho^2A_1A_2^2}{2}\cdot\left[1 - \frac{1}{2}\cos 2\Phi_1\cos 2\alpha_2 + \frac{1}{2}\sin 2\Phi_1\sin 2\alpha_2\right] - \frac{\varepsilon_1\beta_1\omega_1\omega_L\rho A_1^2A_2}{2}\cos(\alpha_2 + \Phi_1) - \omega_1^2\rho A_2\sin(\alpha_2 + \Phi_1) = 0 \tag{16}$$

$$-A_2\omega_L^2\cos\alpha_2 + \varepsilon_2\omega_2A_2\omega_L\sin\alpha_2 - \frac{\varepsilon_2\beta_2\omega_2\omega_LA_2^3}{4}\sin\alpha_2\,\frac{\varepsilon_2\beta_2\omega_2\omega_L\rho^2A_2A_1^2}{2}\cdot\left[\sin\alpha_2 - \frac{1}{2}\sin 2\Phi_1\cos\alpha_2 + \frac{1}{2}\cos 2\Phi_1\sin\alpha_2\right] - \frac{\varepsilon_2\beta_2\omega_2\omega_L\rho A_2^2A_1}{2}\sin(2\alpha_2 - \Phi_1) + \omega_2^2A_2\cos\alpha_2 + \omega_2^2\rho A_1\cos\Phi_1 = 0 \tag{17}$$

$$A_2\omega_L^2\sin\alpha_2 + \varepsilon_2\omega_2A_2\omega_L\cos\alpha_2 - \frac{\varepsilon_2\beta_2\omega_2\omega_L{A_2}^3}{4}\cos\alpha_2 - \frac{\varepsilon_2\beta_2\omega_2\omega_L\rho^2A_2{A_1}^2}{2}\cdot\left[\cos\alpha_2 - \frac{1}{2}\cos 2\Phi_1\cos\alpha_2 - \frac{1}{2}\sin 2\Phi_1\sin\alpha_2\right] - \frac{\varepsilon_2\beta_2\omega_2\omega_L\rho A_2^2A_1}{2}\cos(2\alpha_2 - \Phi_1) - \omega_2^2A_2\sin\alpha_2 - \omega_2^2\rho A_1\sin\Phi_1 = 0. \tag{18}$$

For identical matched active elements the uncoupled amplitudes and frequencies are equal, hence $A_1 = A_2 = A$, $\varepsilon_1 =$

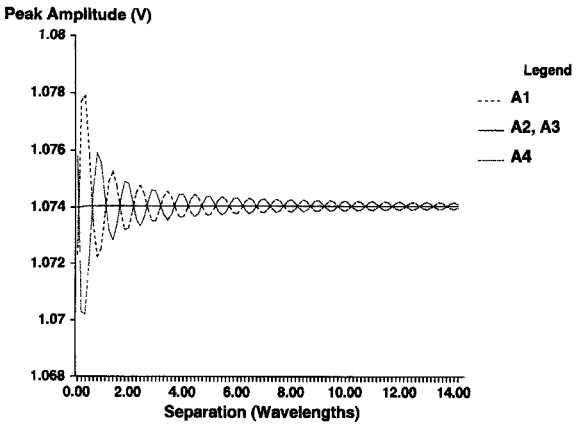

Fig. 8. Amplitude response for four coupled active antenna elements (90° phase progression).

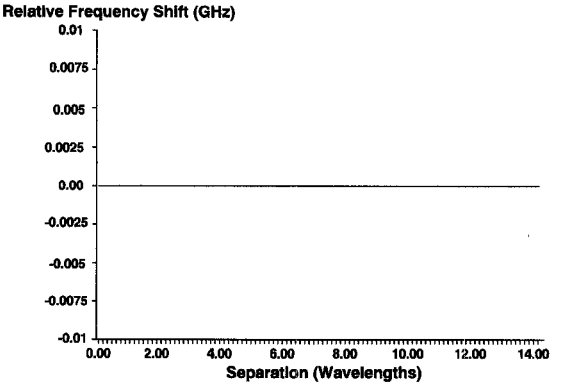

Fig. 9. Frequency response for four coupled active antenna elements (90° phase progression).

$\varepsilon_2 = \varepsilon$, and $\beta_1 = \beta_2 = \beta$ and (15)–(18) reduce to two equations when the condition $\alpha_2 = 0°$ or $\alpha_2 = 180°$ is imposed. The resulting equations can then be solved directly for A and ω_L, the remaining unknowns. This is in agreement with the observations given in [20]. For the case of α_2 set equal to 180° (7) results.

For two elements mutually coupled together in an array, a mode change is observed as separation distance is increased [18]. The preferred stable mode is that which results in the least dissipated power [21]. This can be accounted for by performing a simulation run on both of the allowable mode cases ($\alpha_2 = 0°$ or 180°) and selecting the preferred mode when the peak amplitude of one mode falls below the value it has when operated in the other permitted mode.

VI. Simulation Results

In this section, results based on (A1) and (A2) are presented to illustrate the interesting amplitude and phase phenomena which can occur within a chain array. Due to equipment limitations only simulated results are presented.

The case examined is for four coupled elements, with a progressive phase offset between each element of 90° which is enforced by removing the phase angles, α_2, α_3, and α_4 as optimization variables in (A1) and (A2) (Fig. 8). Here elements one and four track in anti-phase while elements two and three remain invariant with separation distance. Interestingly in this case no frequency variation with separation distance is observed in the simulation (Fig. 9).

In a practical situation knowledge of the behavior of the array with element separation allows optimal spacing information to be assembled with respect to element power generation and operating frequency sensitivity. This information can then be employed as additional constraining factors in the design of active antenna arrays over and above those normally used in classical passive array design techniques.

VII. Conclusion

This paper has illustrated that coupled Van der Pol equations can be derived and analytically solved to determine multiple active antenna amplitude and frequency behavior factors. These equations can be modified to allow for device coupling between a single active antenna and an imaging plate. From the resulting equations the array coupling coefficients can be obtained from a single observation of imaged array operating frequency. When this array coupling factor is fed back to the model the amplitude and entrained frequency response of the actual system can be obtained.

The method can be extended to allow a canonical solution for N-coupled nonidentical unequally spaced elements, and from this the special two element and imaged array cases can be derived.

For the two element array case amplitude and frequency predictions were made. The amplitude and frequency behavior of a system of four active antenna oscillators were simulated and the effects of amplitude and phase tracking discussed. Internal compensation phenomena were observed when more than two elements were used, which can result in zero frequency fluctuation with element separation.

Appendix
N Element Array

Using (8)–(12) it is possible to find two algebraic relationships in $\cos \omega_L t$ and $\sin \omega_L t$ for the nth oscillator. An approximate solution of the form given by equation below is assumed

$$v_n = A_n(\omega_L t + \alpha_n).$$

On following the method of solution adopted previously and by substituting the above equation into (8) we get the two algebraic relationships

$$\begin{aligned}
&-A_n\omega_L^2 \cos\alpha_n + \varepsilon_n\omega_n A_n\omega_L \sin\alpha_n \\
&\quad - \frac{\varepsilon_n\beta_n\omega_n\omega_L A_n^3}{4}\sin\alpha_n - \frac{\varepsilon_n\beta_n\omega_n\omega_L\rho_{n-1}^2 A_n A_{n-1}^2}{2} \\
&\quad \cdot \left[\sin\alpha_n - \frac{1}{2}\sin 2\Phi_{n-1}\cos(2\alpha_{n-1} - \alpha_n)\right. \\
&\quad \left. - \frac{1}{2}\cos 2\Phi_{n-1}\sin(2\alpha_{n-1} - \alpha_n)\right] \\
&\quad - \frac{\varepsilon_n\beta_n\omega_n\omega_L\rho_n^2 A_n A_{n+1}^2}{2} \\
&\quad \cdot \left[\sin\alpha_n - \frac{1}{2}\sin 2\Phi_n\cos(2\alpha_{n+1} - \alpha_n)\right.
\end{aligned}$$

$$
\begin{aligned}
&- \frac{1}{2}\cos 2\Phi_n \sin(2\alpha_{n+1} - \alpha_n)\Big] \\
&- \frac{\varepsilon_n \beta_n \omega_n \omega_L \rho_{n-1} A_n^2 A_{n-1}}{2} \\
&\cdot [\sin(2\alpha_n - \alpha_{n-1} - \Phi_{n-1})] \\
&- \frac{\varepsilon_n \beta_n \omega_n \omega_L \rho_n A_n^2 A_{n+1}}{2} [\sin(2\alpha_n - \alpha_{n+1} - \Phi_n)] \\
&- 2\rho_n \rho_{n-1} \varepsilon_n \beta_n \omega_n \omega_L A_n A_{n-1} A_{n+1} \\
&\cdot \Big\{ -\frac{\cos\alpha_n}{4} [\sin(\alpha_{n-1} + \Phi_{n-1} + \alpha_{n+1} + \Phi_n)] \\
&+ \frac{\sin\alpha_n}{4} [\cos(\alpha_{n-1} + \Phi_{n-1} - \alpha_{n+1} - \Phi_n) \\
&+ 2\cos(\alpha_{n-1} + \Phi_{n-1})\cos(\alpha_{n+1} + \Phi_n)] \Big\} \\
&+ \omega_n^2 A_n \cos\alpha_n + \omega_n^2 \rho_{n-1} A_{n-1} \cos(\alpha_{n-1} + \Phi_{n-1}) \\
&+ \omega_n^2 \rho_n A_{n+1} \cos(\alpha_{n+1} + \Phi_n) = 0 \qquad \text{(A1)}
\end{aligned}
$$

and

$$
\begin{aligned}
&A_n \omega_L^2 \sin\alpha_n + \varepsilon_n \omega_n A_n \omega_L \cos\alpha_n \\
&- \frac{\varepsilon_n \beta_n \omega_n \omega_L A_n^3}{4}\cos\alpha_n - \frac{\varepsilon_n \beta_n \omega_n \omega_L \rho_{n-1}^2 A_n A_{n-1}^2}{2} \\
&\cdot \Big[\cos\alpha_n - \frac{1}{2}\cos 2\Phi_{n-1}\cos(2\alpha_{n-1} - \alpha_n) \\
&+ \frac{1}{2}\sin 2\Phi_{n-1}\sin(2\alpha_{n-1} - \alpha_n)\Big] \\
&- \frac{\varepsilon_n \beta_n \omega_n \omega_L \rho_n^2 A_n A_{n+1}^2}{2} \\
&\cdot \Big[\cos\alpha_n - \frac{1}{2}\cos 2\Phi_n \cos(2\alpha_{n+1} - \alpha_n) \\
&+ \frac{1}{2}\sin 2\Phi_n \sin(2\alpha_{n+1} - \alpha_n)\Big] \\
&- \frac{\varepsilon_n \beta_n \omega_n \omega_L \rho_{n-1} A_n^2 A_{n-1}}{2} \\
&\cdot [\cos(2\alpha_n - \alpha_{n-1} - \Phi_{n-1})] \\
&- \frac{\varepsilon_n \beta_n \omega_n \omega_L \rho_n A_n^2 A_{n+1}}{2} [\cos(2\alpha_n - \alpha_{n+1} - \Phi_n)] \\
&- 2\rho_n \rho_{n-1} \varepsilon_n \beta_n \omega_n \omega_L A_n A_{n-1} A_{n+1} \\
&\cdot \Big\{ -\frac{\sin\alpha_n}{4} [\sin(\alpha_{n-1} + \Phi_{n-1} + \alpha_{n+1} + \Phi_n)] \\
&+ \frac{\cos\alpha_n}{4} [\cos(\alpha_{n-1} + \Phi_{n-1} - \alpha_{n+1} - \Phi_n) \\
&+ 2\sin(\alpha_{n-1} + \Phi_{n-1})\sin(\alpha_{n+1} + \Phi_n)] \Big\} \\
&- \omega_n^2 A_n \sin\alpha_n - \omega_n^2 \rho_{n-1} A_{n-1} \sin(\alpha_{n-1} + \Phi_{n-1}) \\
&- \omega_n^2 \rho_n A_{n+1} \sin(\alpha_{n+1} + \Phi_n) = 0. \qquad \text{(A2)}
\end{aligned}
$$

These can be solved for A_n and α_n by numerical optimization for any integer number of active antenna elements. Mathcad [22] was used to help handle expansion of the identities involved in formulation of (A1) and (A2).

ACKNOWLEDGMENT

The authors would like to thank A. Black and P. Pollock for the construction of the circuits used in this work.

REFERENCES

[1] R. A. York and R. C. Compton, "Measurement and modeling of radiative coupling in oscillator arrays," *IEEE Trans. Microwave Theory Tech.*, vol. 41, no. 3, pp. 438–444, Mar. 1993.
[2] R. J. Dinger, D. J. White, and D. R. Bowling, "10 GHz space power-combiner with parasitic injection-locking," *Electron. Lett.*, vol. 23, pp. 397–398, Apr. 1987.
[3] K. D. Stephan, "Inter-injection-locked oscillators for power combining and phased arrays," *IEEE Trans. Microwave Theory Tech.*, vol. 34, pp. 1017–1025, Oct. 1986.
[4] T. Endo and S. Mori, "Model analysis of a multimode ladder oscillator," *IEEE Trans. Circuits Syst.*, vol. 23, no. 2, pp. 100–113, Feb. 1976.
[5] S. Nogi, J. Lin, and T. Itoh, "Model analysis and stabilization of a spatial power combining array with strongly coupled oscillators," *IEEE Trans. Microwave Theory Tech.*, vol. 41, no. 10, pp. 1827–1837, Oct. 1993.
[6] J. Lin and T. Itoh, "Two-dimensional quasioptical power-combining array using strongly coupled oscillators," *IEEE Trans. Microwave Theory Tech.*, vol. 42, no. 4, pp. 734–741, Apr. 1994.
[7] R. A. York and R. C. Compton, "Quasioptical power combining using mutually synchronized oscillator arrays," *IEEE Trans. Microwave Theory Tech.*, vol. 39, no. 6, pp. 1000–1009, June 1991.
[8] ——, "Experimental observation and simulation of mode-locking phenomena in coupled-oscillator arrays," *J. Appl. Phys.*, vol. 71, no. 6, pp. 2959–2965, Mar. 1992.
[9] J. W. Mink, "Quasioptical power combining of solid-state millimeter-wave sources," *IEEE Trans. Microwave Theory Tech.*, vol. 34, pp. 273–279, Feb. 1986.
[10] A. Balasubramaniyan and A. Mortazawi, "Two-dimensional MESFET-based spatial power combiners," *IEEE Microwave and Guided Wave Lett.*, vol. 3, no. 10, pp. 366–368, Oct. 1993.
[11] V. F. Fusco, S. Drew, and S. D. McDowall, "Synthesis and performance of an active microstrip antenna," in *Special Issue CAD of Printed Antennas and Arrays, Int. J. Microwave and Millimeter Wave Computer Aided Eng.*, vol. 4, no. 1, pp. 100–110, Jan. 1994.
[12] H. Pues and A. Van de Cappelle, "Accurate transmission line model for the rectangular microstrip antenna," *IEE Proc.*, vol. 131, pt. H, no. 6, pp. 334–339, Dec. 1984.
[13] B. Van der Pol, "The nonlinear theory of electrical oscillators," *Proc. IRE*, vol. 22, no. 9, pp. 1051–1086, Sept. 1934.
[14] K. F. Lee and J. S. Dahele, "Characteristics of microstrip patch antennas," in *Handbook of Microstrip Antennas*, J. R. James and P. S. Hall, Eds. London: Peter Peregrinus Ltd., 1989, p. 125.
[15] M. L. Oberhart and Y. T. Lo, "New simple feed network for an array module of four microstrip elements," *Electron. Lett.*, vol. 23, no. 9, pp. 436–437, Apr. 1987.
[16] D. W. Jordan and P. Smith, *Nonlinear Ordinary Differential Equations*. Clarendon, 1990.
[17] R. Adler, "A study of locking phenomena in oscillators," *Proc. IRE*, vol. 34, pp. 351–357, 1946.
[18] K. D. Stephan and S. L. Young, "Mode stability of radiation-coupled inter-injection locked oscillators for integrated phased arrays," *IEEE Trans. Microwave Theory Tech.*, pp. 921–924, May 1988.
[19] D. A. Linkens, "Stability of entrainment conditions for a particular form of mutually coupled Van Der Pol oscillators," *IEEE Trans. Circuits and Syst.*, vol. CAS-23, no. 2, pp. 113–121, Feb. 1976.
[20] J. Lin and T. Itoh, "Mode switch in a two-element active array," in *Proc. 93, IEEE Antennas Propagat. Dig.*, vol. 2, pp. 664–666, June 1993.
[21] M. Kuramitsu and F. Takase, "Analytical method for multimode oscillators using the averaged potential," *Electron. Communicat. Japan*, vol. 66-A, no. 4, pp. 10–19, 1983.
[22] Mathcad, MathSoft Inc., 201 Broadway, Cambridge, MA 02139.

Denver E. J. Humphrey (S'95) was born in Ballymena, N. Ireland, on July 15, 1972. He received the B.Eng. degree from The Queen's University of Belfast, N. Ireland, in 1993.

He is currently a member of the High Frequency Electronics Research Group at Queen's University, where he is carrying out research for his Ph.D. with particular interest on active antenna arrays.

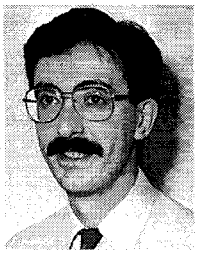

Vincent F. Fusco (M'92) received the Ph.D. degree from The Queen's University of Belfast, N. Ireland.

He has worked as a Research Engineer on short range radar and radio telemetry systems and is currently Reader in Microwave Communications in the School of Electrical Engineering and Computer Science, The Queen's University of Belfast where he is also Head of the High Frequency Electronics Research Group. He is a Chartered Electrical Engineer. His current research interests include nonlinear microwave circuit design and concurrent techniques for electromagnetic field problems. He has published numerous research papers in these areas, and is the author of *Microwave Circuits, Analysis and Computer Aided Design* (Prentice-Hall, 1987).

Stephen Drew received the B.Eng. and the Ph.D. degrees from The Queen's University of Belfast in 1991 and 1995, respectively.

He is currently a Postdoctoral Research Assistant at The Queen's University. His current research interests are active antenna circuits and microwave electronics.